molecules

MDPI

Article

Anti-Inflammatory Activity and ROS Regulation Effect of Sinapaldehyde in LPS-Stimulated RAW 264.7 Macrophages

Seung-Hwa Baek [1,2], Tamina Park [1,3], Myung-Gyun Kang [1] and Daeui Park [1,2,3,*]

[1] Department of Predictive Toxicology, Korea Institute of Toxicology, Daejeon 34114, Korea; seunghwa.beak@kitox.re.kr (S.-H.B.); tamina.park@kitox.re.kr (T.P.); myung-gyun.kang@kitox.re.kr (M.-G.K.)

[2] Center for Convergent Research of Emerging Virus Infection, Korea Research Institute of Chemical Technology, Daejeon 34114, Korea

[3] Department of Human and Environmental Toxicology, University of Science and Technology, Daejeon 34113, Korea

* Correspondence: daeui.park@kitox.re.kr; Tel.: +82-42-610-8844

Academic Editor: Seyed Khosrow Tayebati

Received: 24 August 2020; Accepted: 3 September 2020; Published: 7 September 2020

Abstract: We evaluated the anti-inflammatory effects of SNAH in lipopolysaccharide (LPS)-stimulated RAW 264.7 macrophages by performing nitric oxide (NO) assays, cytokine enzyme-linked immunosorbent assays, Western blotting, and real-time reverse transcription-polymerase chain reaction analysis. SNAH inhibited the production of NO (nitric oxide), reactive oxygen species (ROS), tumor necrosis factor (TNF)-α, and interleukin (IL)-6. Additionally, 100 μM SNAH significantly inhibited total NO and ROS inhibitory activity by 93% ($p < 0.001$) and 34% ($p < 0.05$), respectively. Protein expression of inducible nitric oxide synthase (iNOS) and cyclooxygenase-2 (COX-2) stimulated by LPS were also decreased by SNAH. Moreover, SNAH significantly ($p < 0.001$) downregulated the TNF-α, IL-6, and iNOS mRNA expression upon LPS stimulation. In addition, 3–100 μM SNAH was not cytotoxic. Docking simulations and enzyme inhibitory assays with COX-2 revealed binding scores of −6.4 kcal/mol (IC_{50} = 47.8 μM) with SNAH compared to −11.1 kcal/mol (IC_{50} = 0.45 μM) with celecoxib, a known selective COX-2 inhibitor. Our results demonstrate that SNAH exerts anti-inflammatory effects via suppression of ROS and NO by COX-2 inhibition. Thus, SNAH may be useful as a pharmacological agent for treating inflammation-related diseases.

Keywords: sinapaldehyde; anti-inflammatory effect; nitric oxide; reactive oxygen species; cytokine; docking simulation

1. Introduction

Inflammatory reactions typically occur as a natural physiological response against injurious stimuli such as the infectious invasion of pathogens and toxins [1]. However, uncontrolled and aberrant inflammation leads to many diseases such as rheumatoid arthritis [2], atherosclerosis [3], asthma [4], diabetes [5], chronic hepatitis [6], septic shock [7], and inflammatory neurodegenerative diseases [8]. During chronic inflammation, activated macrophages secrete high chemokines (interleukin-8 [IL-8], CC-chemokine ligand 5 [CCL 5], eotaxin), cytokines (tumor necrosis factor-alpha [TNF-α], IL-1α, IL-1β, IL-6, granulocyte-macrophage colony-stimulating factor [GM-CSF]), and pro-inflammatory mediators (nitric oxide [NO], inducible nitric oxide synthase [iNOS], cyclooxygenase-2 [COX2]) [9].

Lipopolysaccharide (LPS) is widely localized in the outer cell wall of Gram-negative bacteria. Thus, LPS elicits a host inflammatory response that results in increased production of chemokines, cytokines, and pro-inflammatory mediators by the immune system [10]. Macrophages exposed to LPS

during microorganism infections stimulate the immune system to produce cytokines and chemokines, followed by inflammatory events. Thus, inhibiting macrophage activation by LPS is an important focus for therapeutic strategies aimed at treating inflammatory diseases [11–14].

Reactive oxygen species (ROS) are natural byproducts of oxygen metabolism that play important roles in cell signaling and homeostasis [15]. However, under various infection and pathological conditions, excess ROS production can cause protein and nucleic acid oxidation and can lead to toxic effects on cell structures [16]. Recent studies suggest that ROS can lead to activation of inflammatory effects via the mitogen-activated protein kinase (MAPK) signaling pathway, which induces the production of numerous inflammatory cytokines [17–20].

Sinapaldehyde (SNAH) is a methoxyphenol found in several plants such as *Senra incan* [21], *Ailanthus altissima* Swingle [22], *Eucalyptus globulus* [23], *Oryza sativa* [24], *Dendropanax dentiger* [25], and *Populus tomentosa* [26]. It was reported that SNAH exerts antibacterial activities against oral pathogenic bacteria, including *Streptococcus pyogenes*, *Streptococcus mitis*, and *Streptococcus mutans* [27]. Additionally, SNAH dose-dependently decreases ethyl phenylpropiolate-induced edema in the rat ear [21]. However, to our knowledge the anti-inflammatory effects of SNAH have not been examined; thus, the objective of this study was to investigate the anti-inflammatory activity of SNAH in macrophage RAW 264.7 cells. We investigated the effects of SNAH on cytokine (TNF-α and IL-6) production and its impact on the expression of COX-2 and iNOS proteins and TNF-α, iNOS, and IL-6 genes in LPS-induced RAW 264.7 cells. Furthermore, COX2 inhibitory effects of SNAH were analyzed using molecular docking simulation and enzyme inhibitory assays.

2. Results

2.1. Effect of SNAH on Cell Viability and LPS-Induced NO Production in RAW 264.7 Cells

The cytotoxic effect of SNAH was examined using XTT (Cell Proliferation Kit II) assay. For SNAH concentrations ranging from 1–100 μM, cell viability was not significantly changed after 18-h treatment with 1 μg/mL LPS compared to control group cells. Flow cytometry is a sensitive method for detecting altered cell cytotoxicity. Propidium iodide penetrates the leaky membrane of dead/dying cells and binds DNA. Thus, it is widely used in flow cytometry assays [28]. Up to 100 μM, SNAH did not cause significant cytotoxicity (Figure 1d). Therefore, subsequent experiments were conducted at SNAH concentrations up to 100 μM. On the other hand, apigenin [29,30] and genistin [31], which are standard substances extracted from natural plants with anti-inflammatory activity, showed cytotoxicity at a concentration of 100 μM, and the experimental concentration was determined to be 30 μM. The effect of SNAH on NO production in LPS-induced RAW 267.4 cells was confirmed in a Griess reagent assay. LPS treatment significantly elevated ($p < 0.05$) the NO level by 18-fold. In contrast, treatment with 100 μM SNAH significantly inhibited NO production in RAW 264.7 cells stimulated with LPS. SNAH at 3, 10, 30, and 100 μM dramatically decreased NO formation by 29% ± 6.1%, 56% ± 2.8%, 72% ± 4.0%, and 93% ± 1.1%, respectively, compared to LPS-stimulated control cells (Figure 1b). However, apigenin and genistin decreased NO production by 55% ± 5.2% and 50% ± 3.0% activity, respectively, at 30 μM concentration (Figure 1c).

2.2. Effects of SNAH on Cytokine Production in RAW 264.7 Cells

Next, we measured the effect of SNAH on the expression of IL-6 and TNF-α in the supernatant of LPS-treated RAW 264.7 cells via enzyme-linked immunosorbent assay (ELISA). In cultures of LPS-treated cells, IL-6 and TNF-α concentrations were significantly increased. The LPS-induced increases were dose-dependently reversed by SNAH treatment. As shown in Figure 2, 30–100 μM SNAH significantly suppressed the production of IL-6 and TNF-α. The release of TNF-α and IL-6 was reduced by up to 59% ± 1.1% and 64% ± 3.5%, respectively, compared to LPS-stimulated control cells.

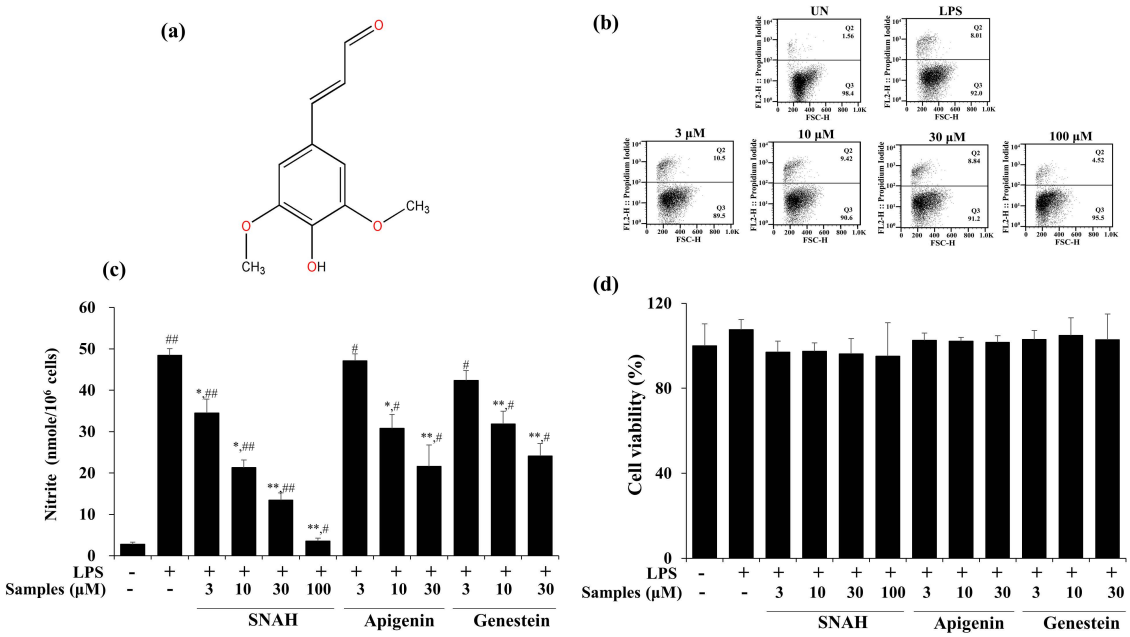

Figure 1. Effects of SNAH (sinapaldehyde) on cell viability and LPS (lipopolysaccharide)-induced NO (nitric oxide) production in RAW 264.7 cells. (**a**) The chemical structure of SNAH. (**b**) The viability of Raw264.7 cells was determined by FACS (fluorescence activated cell sorter) analysis. (**c**) Cells were pretreated with 3, 10, 30, and 100 μM SNAH for 1 h before treatment with 1 μg/mL LPS. After incubation for 18 h, NO production was detected by Griess test. (**d**) The cell viability was detected by XTT assay. The values are presented as means ± SD of three independent experiments. * $p < 0.05$, ** $p < 0.01$, compared to the LPS-treated group. # $p < 0.05$, ## $p < 0.01$, compared to the LPS non-treated group.

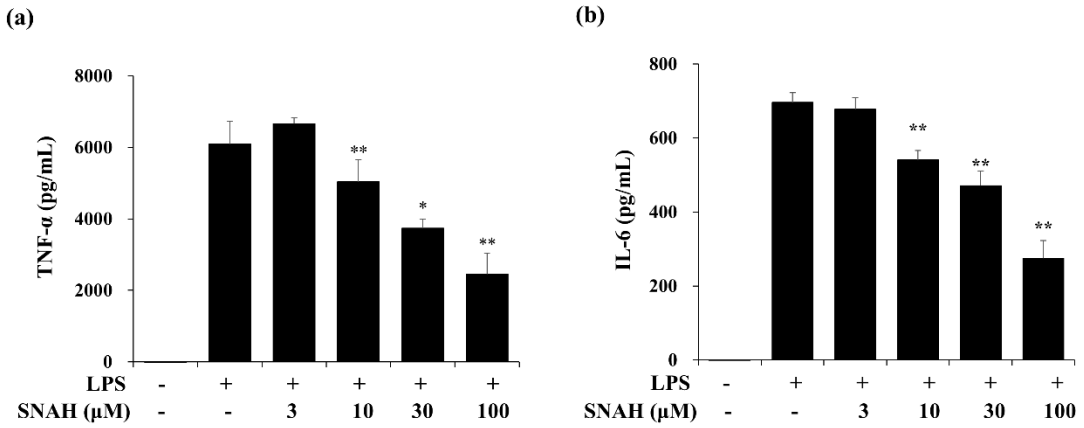

Figure 2. Effects of SNAH on LPS-induced TNF-α (**a**) and IL-6 (**b**) production. RAW 264.7 cells were pretreated with 3, 10, 30, and 100 μM SNAH for 1 h before treatment with 1 μg/mL LPS. After incubation for 18 h, IL-6 and TNF-α production was detected by ELISA. The values are presented as means ± SD of three independent experiments. * $p < 0.05$, ** $p < 0.01$ compared to the LPS-treated group.

2.3. Effects of SNAH on iNOS and COX-2 Expression in RAW 264.7 Cells

We examined the effects of SNAH on the expression of inflammatory factors in LPS-stimulated RAW 264.7 cells. Western blot analysis showed that 100 μM SNAH treatment decreased iNOS and COX-2 protein expression by 94% ± 1.2% and 82% ± 3.2%, respectively, compared to the LPS-stimulated control cells (Figure 3).

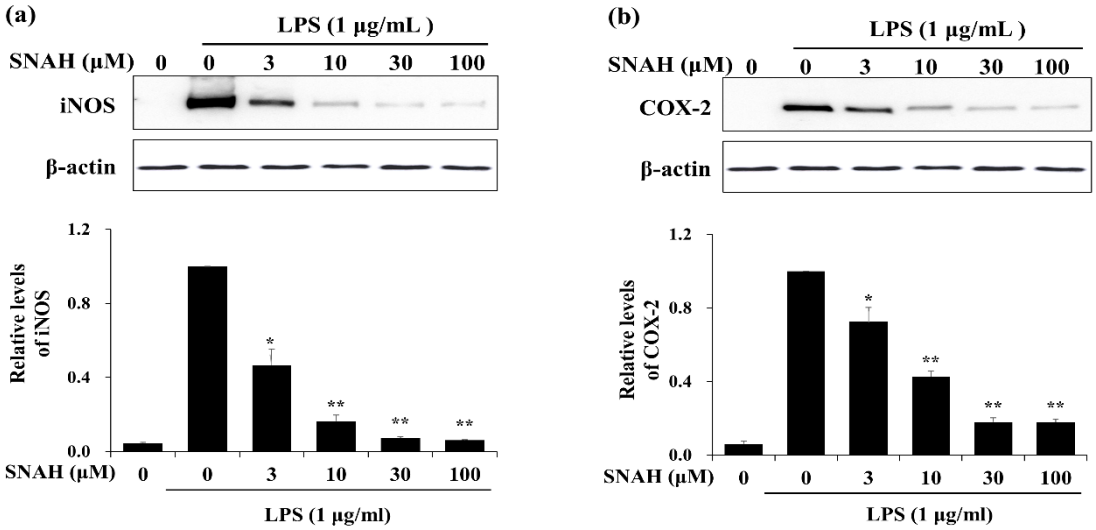

Figure 3. Effects of SNAH on LPS-induced iNOS and COX-2 protein expression. RAW 264.7 Cells were pretreated with 3-100 μM SNAH for 1 h before treatment with 1 μg/mL LPS. After incubation for 24 h, iNOS (**a**) and COX-2 (**b**) protein levels were detected by Western blot. The values are presented as means ± SD of three independent experiments. * $p < 0.05$, ** $p < 0.01$ compared to the LPS-treated group.

2.4. Effects of SNAH on Inflammatory Gene Expression in RAW 264.7 Cells

To determine the effects of SNAH on LPS-induced expression of pro-inflammatory cytokines, mRNA levels of TNF-α, IL-6, and iNOS in RAW 264.7 cells were measured by real-time RT-PCR. As shown in Figure 4, LPS stimulation significantly increased the expression of TNF-α, IL-6, and iNOS mRNA compared to the control group in the absence of LPS. In contrast, IL-6, TNF-α, and iNOS mRNA were significantly ($p < 0.01$) downregulated by SNAH treatment. At 10, 30, and 100 μM, SNAH significantly ($p < 0.01$) inhibited iNOS mRNA expression by 39% ± 2.1%, 83% ± 1.8% and 92% ± 0.3% ($n = 5$), respectively, compared to LPS-stimulated control cells. The mRNA levels of pro-inflammatory cytokines IL-6 and TNF-α significantly ($p < 0.01$) decreased 74% ± 2.7% and 82% ± 3.6% ($n = 5$), respectively, compared to LPS-stimulated control cells.

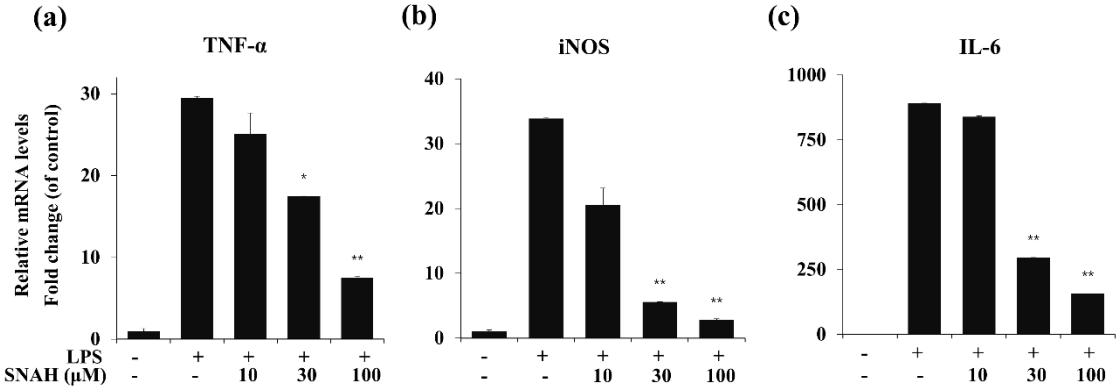

Figure 4. Effect of SNAH on TNF-α, iNOS, and IL-6 gene expression in RAW 264.7 cells. RAW264.7 cells were pretreated with 10-100 μM SNAH for 1 h prior to LPS stimulation. After 6h LPS stimulation, total RNA was isolated using Trizol reagent. TNF-α (**a**), iNOS (**b**), and IL-6 (**c**) mRNA levels were analyzed by real-time RT-PCR. Relative mRNA levels were determined using the Ct-value method and normalized to GAPDH expression. The values are presented as means ± SD of three independent experiments. * $p < 0.05$, ** $p < 0.01$ compared to the LPS-treated group.

2.5. Effect of SNAH on ROS Production in RAW 264.7 Cells and Radical Scavenging Activity

Next, we investigated the effect of SNAH on ROS formation in LPS-treated RAW 264.7 macrophages. LPS treatment elevated intracellular ROS levels in macrophages after 24 h. In contrast, SNAH treatment significantly reduced LPS-induced ROS production in a dose-dependent manner. Treatment with 10, 30, and 100 μM SNAH significantly ($p < 0.01$) decreased ROS generation by 39% ± 3.1%, 64% ± 9.8%, and 78% ± 2.1%, respectively, compared to LPS-stimulated control cells (Figure 5). These findings suggest that the anti-inflammatory effect of SNAH is associated with its antioxidant effects in RAW 264.7 cells. To check the radical scavenging activity of SNAH, the DPPH radical-scavenging activity of the SNAH was carried out using ascorbic acid as a reference compound. At a concentration of 250 μM, SNAH identified radical scavenging effects of 73% ± 2% compared with 72% ± 2% for ascorbic acid. The amount of the SNAH necessary to decrease the DPPH radical by 50% (IC_{50}) was calculated, and it was found that SNAH confirmed activity with a radical-scavenging effect of 172 μM compared with ascorbic acid (IC_{50} of 192 μM) (Table 1). Therefore, the ability of SNAH to strongly suppress ROS in LPS-stimulated RAW 264.7 macrophages might be associated with its ability to scavenge free radicals.

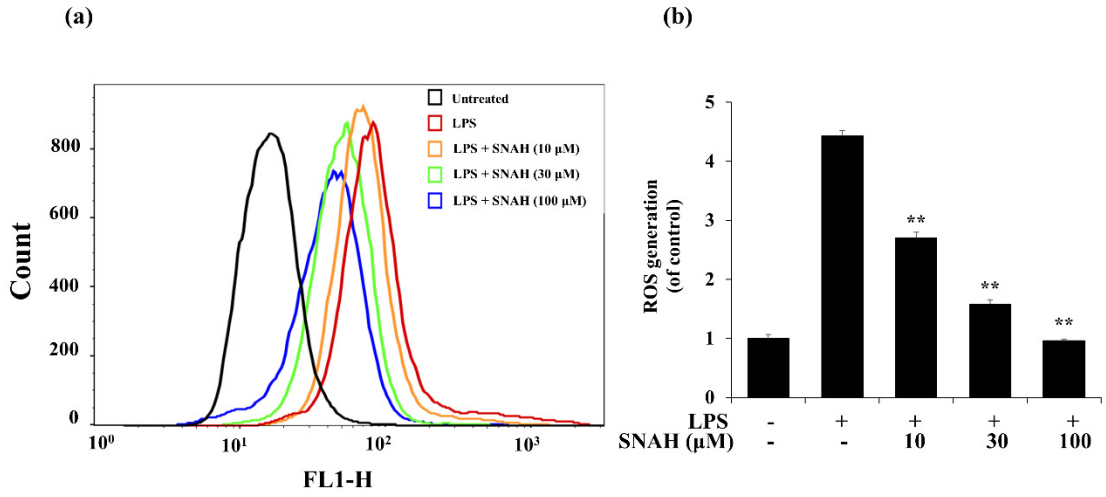

Figure 5. Effects of SNAH on LPS-induced ROS (reactive oxygen species) production. (**a**) RAW 264.7 cells were pretreated with 10–100 μM SNAH for 1 h before treatment with 1 μg/mL LPS for 18 h. Cells were incubated with 10 μM 2′,7′-dichlorofluorescein diacetate (DCFH-DA) for 30 min at 37 °C. Then, cells were harvested, and dichlorofluorescein (DCF) fluorescence was immediately analyzed by flow cytometry. DCF fluorescence intensity was determined from the same numbers of cells in a randomly selected area. (**b**) The mean relative ROS level is presented in a bar graph. The values are presented as means ± SD of three independent experiments ** $p < 0.01$, compared to the LPS-treated group.

Table 1. DPPH radical-scavenging activity of the SNAH and IC_{50} values.

Compounds	DPPH [1] Radical Scavenging Activity (%)				IC_{50} (μM)
	62.5 μM	125 μM	250 μM	500 μM	
SNAH	25% ± 5% [2]	48% ± 2%	73% ± 2%	87% ± 1%	172
Ascorbic acid	19% ± 1%	49% ± 5%	72% ± 2%	84% ± 3%	192

[1] 2,2′-diphenyl-1-picrylhydrazyl; [2] Values are expressed as mean ± SD of triplicate determinations.

2.6. Effect of SNAH on MAPK and p65 Signaling in RAW 264.7 Cells

When RAW 264.7 cells were exposed to LPS, the phosphorylated ERK and SAPK/JNK (stress-activated protein kinase/Jun-amino-terminal kinase) increased in a time-dependent manner (Figure 6). Phosphorylated ERK1/2 was decreased in the presence of SNAH at 10 min. Moreover, SNAH treatment decreased SAPK/JNK phosphorylation after 20 min. In addition, phosphorylated p65

was induced in the LPS-stimulated group, while *p*-p65 decreased in the SNAH-treated group. At 10, 30, and 100 μM, SNAH inhibited p65 phosphorylation by 40%, 39%, and 57%, respectively, compared to LPS-stimulated control cells.

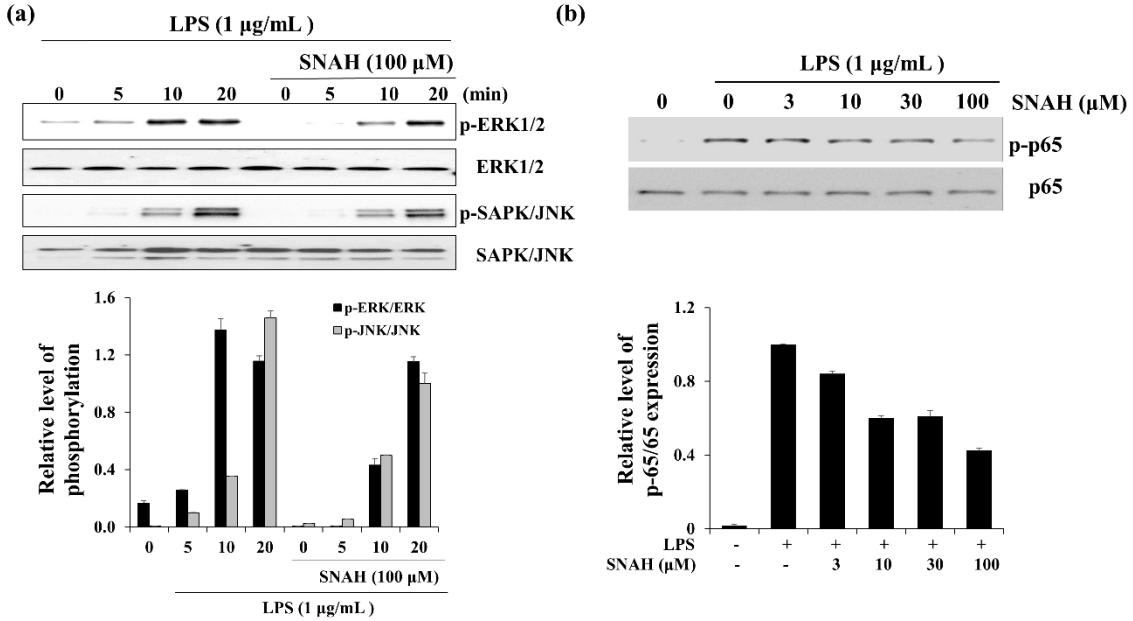

Figure 6. Effect of SNAH on MAPK and p65 signaling pathways. (**a**) The time course of ERK (extracellular-signal-regulated kinase) and SAPK/JNK (Stress-activated protein kinase/Jun-amino-terminal kinase) phosphorylation stimulated by LPS in RAW264.7 cells. (**b**) RAW 264.7 cells were treated for 15 min with LPS (1 μg/mL) alone or with LPS (1 μg/mL) coupled with 3–100 μM SNAH. Cell lysates were prepared and blotted with the indicated anti-phospho-antibodies. Total ERK1/2, SAPK/JNK, and NF-κB (p65) were probed as quantitative controls.

2.7. Molecular Docking Studies and COX-2 Enzyme Inhibitory Activity

Docking simulations showed that SNAH was located properly at binding sites of COX-2. The docking score of SNAH for COX-2 was −6.4 kcal/mol, as measured by AutoDock Vina (Figure 7a). Celecoxib was used as positive control at the same COX-2 binding sites. The docking score of celecoxib was −11.1 kcal/mol. From the docking results, SNAH overlapped with the 4-methylpenyl ring of celecoxib in the binding pocket (Figure 7a). In addition, celecoxib had three hydrogen bond interactions with Leu352, Ser353, and Phe518 of COX-2. However, there were no hydrogen bond interactions between COX-2 and SNAH (Figure 7a).

The next study analyzed COX-2 enzyme inhibition activity of SNAH using COX-2 inhibitory assays. SNAH displayed selective inhibitors to COX-2 with IC_{50} values of 37 μM. The selectivity index (SI value) was calculated as the ratio of concentration (IC_{50}) that inhibits the COX1 and COX2 isoforms [32]. SNAH and celecoxib displayed SI values of >2.7 and >6.25, respectively (Figure 7b). The results of COX inhibition assay indicated that SNAH had a reasonable inhibitory activity against COX-2. Further, SNAH showed no inhibition for COX-1 up to 100 μM. Therefore, our results indicate that SNAH interacts with COX-2 and is a potential COX-2 inhibitor.

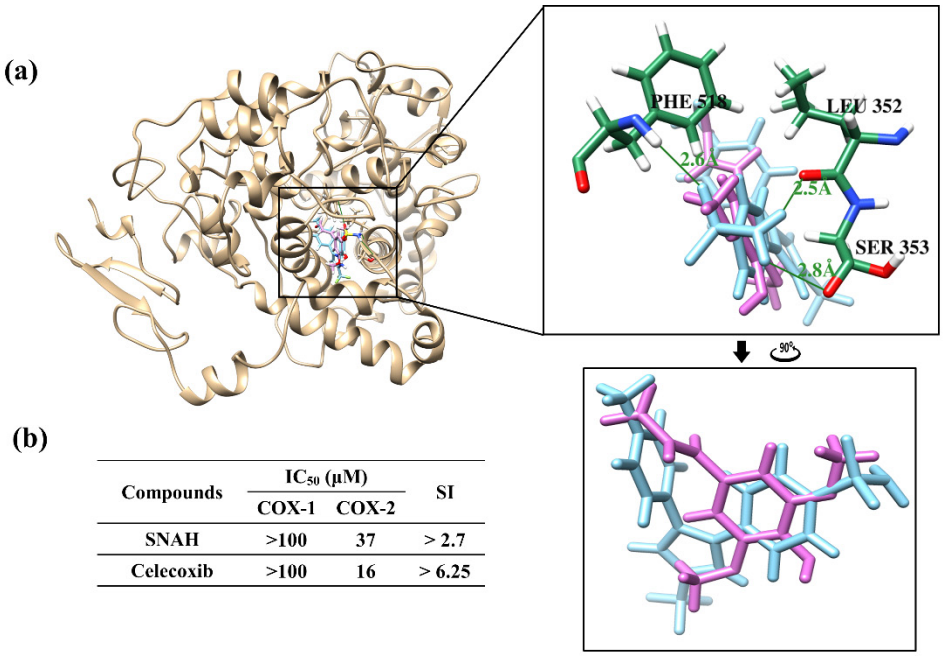

(b)

Compounds	IC_{50} (μM)		SI
	COX-1	COX-2	
SNAH	>100	37	> 2.7
Celecoxib	>100	16	> 6.25

Figure 7. Docking simulation between SNAH and COX-2 (6COX). (**a**) The pink-colored chemical structure represents SNAH, and the COX-2 protein structure complexed with celecoxib is indicated by blue colored. The magnified rectangles indicate the active sites of COX-2 proteins. In the box image, hydrogen bond interactions between COX-2 and SNAH are depicted by green-colored lines. The binding energies of SNAH and celecoxib for COX-2 were −6.4 kcal/mol and −11.1 kcal/mol, respectively. (**b**) COX-2 enzyme inhibitory activities of SNAH. The commercial standard, celecoxib was used as a positive control at identical concentrations.

3. Discussion

The progression of inflammation is the main cause of many disease conditions, including headache, atopy, metabolic syndrome, multiple sclerosis, Alzheimer's disease, and Parkinson's disease [33–35]. When cells are infected by Gram-negative bacteria, LPS in the outer membrane of Gram-negative bacteria activates macrophages, thereby causing them to secrete high concentrations of pro-inflammatory cytokines, and inflammatory factors or mediators. Therefore, LPS-induced inflammatory effects in macrophages are widely utilized to screen anti-inflammatory agents [36]. Macrophage stimulation by LPS promotes excessive NO release via degradation of L-arginine. When responding to inflammatory stimuli in the mammalian immune system, NO generation is regulated by iNOS in macrophage cells [37]. In addition, LPS-induced macrophages produce excess inflammatory mediators, including COX2, a key enzyme in PGE_2 synthesis, and inflammatory cytokines such as TNF-α and IL-6 [38]. There are data changes at each time point of the LPS-induced inflammatory mediator [39]. Firstly, the stimulus of LPS caused the immediate release of TNF-α until 12 h, and then IL-6 was reached a peak at 18 h. The iNOS expression showed a similar change comparing with IL-6. The change of NO release was influenced by the iNOS contents [40]. Therefore, they are the targets of anti-inflammatory reagents in this study. SNAH reduced the production of NO, TNF-α, and IL-6 in LPS-stimulated RAW 264.7 cells in a dose-dependent manner (Figure 2). Moreover, NO inhibitory activity of SNAH was higher than that of apigenin and genistein, standard substances, under the same conditions (Figure 1c).

Nitric oxide synthases (NOSs) exist in three isoforms: endothelial NOS (eNOS), neuronal NOS (nNOS), and iNOS [41]. eNOS and nNOS are constitutively expressed, while iNOS is expressed in response to inflammatory stimuli [42]. iNOS is especially activated in response to inflammatory stimuli such as cytokines, interleukins, and bacterial endotoxin [43]. Cyclooxygenase (COX) exists in two isoforms: COX-1 and COX-2. COX-1 is a constitutively expressed enzyme with general housekeeping functions [44]. COX-2 is an inducible enzyme that catalyzes the biosynthesis of PGE2,

which contributes to the pathogenesis of various inflammatory diseases. PGE2 synthesis is catalyzed by the COX enzyme which is expressed during all inflammatory processes [45]. In inflammatory cells including macrophages, COX-2 and iNOS are induced by inflammatory stimuli such as LPS, resulting in the aggravated cellular inflammatory signaling. iNOS and COX-2 are key enzymes that are involved in NO and PGE2 synthesis, respectively. Therefore, they are the major targets of anti-inflammatory agents in current research [46–48]. Our results showed that SNAH exerts its anti-inflammatory effects by inhibiting iNOS and COX-2 protein expression (Figure 3). Additionally, SNAH regulates iNOS expression at both the protein and gene levels (Figure 4). These findings indicate that SNAH may effectively attenuate inflammatory responses by decreasing NO production via the inhibition of iNOS and COX-2 protein expression, mRNA levels, and pro-inflammatory cytokines secretion.

ROS accumulation from the endogenous antioxidant reaction results in a redox imbalance that leads to oxidative stress [49]. Increased ROS production is strongly associated with many other pathological conditions, such as inflammation. Inflammatory mediators and cytokines promote an influx of macrophages that, in turn, accelerate intracellular ROS accumulation [50]. In addition, ROS act as secondary messengers and participate in the inflammatory signaling pathway [51]. Therefore, the ability of SNAH to strongly suppress ROS in LPS-stimulated RAW 264.7 macrophages might be attributed to its ability to scavenge free radicals (Table 1). SNAH-mediated inhibition of ROS generation may also potentially inhibit the expression of pro-inflammatory mediators and cytokines, thereby explaining the strong anti-inflammatory properties of SNAH.

Many studies indicate that the toll-like receptor (TLR) family of pattern recognition receptors include central mediators of the inflammatory response. Accumulating evidence indicates that TLR4 specifically mediates LPS-induced signaling [52]. The first step in the LPS/TLR4-mediated inflammatory signaling pathway is the binding of LPS to TLR4 complexed with MYD88 adapters at the plasma membrane. This binding initiates intracellular signaling cascades. Activation of TLR4 by LPS induces PI3K/Akt, MAPK, and IB kinase complex phosphorylation, eventually resulting in the activation of NF-κB [53,54]. Further studies are necessary to elucidate the molecular mechanism by which SNAH exerts its inhibitory effects by evaluating the role of TLR-4/MAPK/NF-κB pathway activation.

Docking simulations showed that binding scores obtained from SNAH and celecoxib were correlated with IC_{50} values. Two compounds had similar binding orientations, with overlap between the dimethoxyphenyl ring of SNAH and the 4-methylpenyl ring of celecoxib in the same binding pocket. The pocket site forms an important hydrophobic cavity for the 4-methylpenyl ring of celecoxib to bind COX-2 [55]. Celecoxib forms hydrogen bonds with COX-2 at Leu352, Ser353, and Phe513. We suggest that those hydrogen bonds could increase the binding affinity with COX-2, and that the modification of the SNAH dimethoxyphenyl ring might improve COX-2 inhibition because the substitution of methoxy group at *para* position was responsible for its high potency against COX-2 and high selective index [56].

4. Materials and Methods

4.1. Materials

Dimethyl sulfoxide, apigenin, genistein, LPS (from an *Escherichia coli* strain), 2,7-dichlorofluorescein diacetate (DCF-DA), Griess reagent, and the Cell Proliferation Kit II (XTT) were obtained from Sigma (St. Louis, MO, USA). Dulbecco's Modified Eagle's Medium (DMEM), fetal bovine serum, penicillin (100 IU/mL)-streptomycin (100 μg/mL), and trypsin-EDTA were purchased from Gibco (Grand Island, NY, USA). The ELISA kits for TNF-α and IL-6 were purchased from R&D Systems, Inc. (Minneapolis, MN, USA). Antibodies against *p*-ERK1/2, ERK1/2, *p*-SAPK/JNK, SAPK/JNK, iNOS, COX2, and β-actin, and secondary antibodies were purchased from Cell Signaling Technology (Danvers, MA, USA). SNAH was obtained from ChemFaces Biochemical Co. Ltd. (Wuhan, China), and the purity of SNAH was ≥98%. It was dissolved at a concentration of 100 mM in dimethyl sulfoxide. The IUPAC nomenclature of SNAH is (*E*)-3-(4-hydroxy-3,5-dimethoxyphenyl)acrylaldehyde, and the chemical structure was drawn using ChemDraw software (https://www.perkinelmer.com/category/chemdraw).

4.2. Cell Culture

RAW 264.7 macrophages were obtained from the American Type Culture Collection (Manassas, VA, USA). The cells were grown at 37 °C in DMEM supplemented with 10% fetal bovine serum and penicillin sulfate in a humidified 5% CO_2 atmosphere. The cells were pretreated with SNAH for 1 h, and then stimulated with 1 μg/mL LPS for the indicated time.

4.3. Cell Viability Assay

Cell viability studies were performed using the XTT assay. RAW 264.7 cells were plated at a density of 5×10^5 cells/mL in a 96-well plate, pretreated with isolated SNAH for 1 h, and stimulated with 1 μg/mL LPS for 24 h. XTT assay was measured using a Cell Proliferation Assay Kit II (Roche, Basel, Switzerland). Briefly, the XTT labeling mixture was prepared by mixing 50 volumes 1 mg/mL sodium 3′-[1-(phenylaminocarbonyl)-3,4-tetrazolium]-bis(4-methoxy-6-nitro) benzene sulfonic acid hydrate (in media) with 1 volume 0.383 mg/mL *N*-methyldibenzopyrazine methyl sulfate in PBS. This mixture was added to the cultures and incubated for 1 h at 37 °C. Absorbance was measured at 490 nm with a reference wavelength at 650 nm. The cell viability results were presented as a ratio relative to untreated (UN) samples. For fluorescence-activated cell sorting analysis, the cells were washed in PBS and stained with 0.05 μg propidium iodide for 15 min at room temperature. Flow cytometry analysis was performed on a BD FACSCalibur (BD Biosciences, Franklin Lakes, NJ, USA) using FlowJo (TreeStar, Ashland, OR, USA) and Diva software. Viability was calculated by comparing treated cells to non-treated cells.

4.4. Measurement of Nitric Oxide Production

RAW 264.7 cells were seeded into 96 well plates at a density of 5×10^5 cells/mL for 24 h. The medium was replaced with fresh medium containing 1 μg/mL LPS and 3–100 μM SNAH in the test group, followed by incubation for 24 h. Nitrite accumulated in the culture supernatant was measured as an indicator of NO production using Griess reagent. The culture supernatant was mixed with equal volumes Griess reagent (1% (*w*/*v*) sulfanilamide in 5% (*v*/*v*) phosphoric acid and 0.1% (*w*/*v*) naphthylethylenediamine-HCl) for 10 min. Absorbance at 540 nm was measured in a microplate spectrophotometer (Bio-Tek, Vermont, VT, USA). Fresh culture medium was used as the blank in all experiments. The amount of nitrite in the samples was determined by referring to a sodium nitrite standard curve.

4.5. Measurement of Cytokines by ELISA

The secretion of pro-inflammatory cytokines, including IL-6 and TNF-α, was measured with an ELISA assay kit (R&D Systems, Minneapolis, MN, USA). RAW 264.7 cells were seeded into a 96-well plate containing 3–100 μM SNAH with or without 0.2 μg/mL LPS for 6 h. The supernatant was harvested, and pro-inflammatory cytokine levels were determined using ELISA kits. Absorbance was measured at 450 nm using a microplate spectrophotometer (Bio-Tek). The quantities of cytokines secreted by RAW 264.7 cells were calculated using standard curves.

4.6. Western Blot Analysis

iNOS, COX-2, phospho-ERK1/2, SAPK/JNK, and actin protein expression was determined by Western blotting. RAW 264.7 cells were cultured in 6-well plates (6×10^5 cells/well) with or without 3–100 μM SNAH and 1 μg/mL LPS for 24 h. Cells were lysed with RIPA (radioimmunoprecipitation assay) buffer [50 mM Tris-Cl (pH 8.0), 5 mM EDTA, 150 mM NaCl, 1% NP-40, 0.1% SDS and 1 mM phenylmethylsulfonyl fluoride]. Lysates were centrifuged at 12,000 rpm for 20 min. Supernatants were collected and protein concentrations were determined using a Bio-Rad Protein Assay kit (Bio-Rad Laboratories, Inc., Hercules, CA, USA). Equal amounts of proteins were resolved by 10% SDS-polyacrylamide gel electrophoresis and transferred to nitrocellulose membranes. The membranes

were incubated with blocking buffer (Tris-buffered saline containing 0.2% Tween-20 and 5% non-fat dried milk) and probed with the indicated primary antibodies. After washing, membranes were probed with horseradish peroxidase-conjugated secondary antibodies. Detection was performed using an enhanced chemiluminescence protein detection system (Amersham Biosciences, Little Chalfont, UK). The chemiluminescent signal was detected by 10–120 s exposure using a ChemiDoc Touch Gel Imaging System (Cat. No. 1708370, Bio-Rad, Hercules, CA, USA). Western blotting analyses were repeated three times, and representative results are shown.

4.7. Measurement of Intracellular Reactive Oxygen Species Formation

Intracellular ROS levels were quantified using a ROS-sensitive fluorescence indicator, DCFH-DA. In viable cells, 2,7-dichlorofluorescein diacetate (DCFH-DA) is cleaved to DCFH by esterase, followed by ROS oxidation to form a highly fluorescent molecule, DCF. Briefly, RAW 264.7 cells were plated at a density of 5×10^5 cells/mL in a 6-well plate, pretreated with isolated SNAH for 1 h, and stimulated with 1 μg/mL LPS for 24 h. Then, they were washed twice with 1 × washing buffer and loaded with 10 μM DCFH-DA detection reagent. After incubation in darkness for another 30 min at 37 °C, cells were washed twice with 1 × washing buffer. Fluorescence representing intracellular ROS levels was measured at 485/20 nm excitation and 528/20 nm emission in a fluorescence multi-detection reader (Glomax, Promega, Madison, WI, USA). FACS data were measured with a BD FACSCalibur (BD Biosciences, San Jose, CA, USA) at the excitation wavelength of 488 nm and the emission wavelength of 525 nm. Data were analyzed by FlowJo software (Tree Star, San Carlos, CA, USA).

4.8. DPPH Radical Scavenging Assay

The DPPH radical scavenging assay was conducted using the published protocol method [57]. Briefly, the compound (100 μL) was added to 100 μL of 2 mM DPPH solution in 50% ethanol. The mixtures were mixed well and incubated in the dark for 30 min. The reduction of DPPH absorption was measured at 520 nm using a microplate spectrophotometer (Bio-Tek). Ascorbic acid (100 μM) was used as a positive control. All determinations were performed in triplicate. The DPPH radical scavenging activity was calculated using Equation (1):

$$\text{DPPH scavenging (\%)} = [1 - (\text{Absorbance of the sample/Absorbance of the control})] \times 100 \quad (1)$$

4.9. Real-Time Reverse Transcription-Polymerase Chain Reaction (RT-PCR) Analysis

Total RNA was extracted using an RNeasy Mini Kit (QIAGEN, Valencia, CA, USA) and cDNA was synthesized using AccuPower RT PreMix (BIONEER Corporation, Daejeon, Korea). SYBR Green PCR Master Mix (Life Technologies Corporation, Carlsbad, CA, USA) and an ABI 7500 Sequence Detection System (Applied Biosciences, Foster City, CA, USA) were used for real-time PCR analysis. Primer sequences used in this study are listed in Table 1. Samples were amplified by 40 cycles of 15 s at 95 °C and 1 min at 60 °C. All reactions were run in triplicate, and relative expression levels were determined with the $2^{-\Delta\Delta CT}$ method by normalizing the expression levels to GAPDH. The primer list is in Table 2.

Table 2. List of primers used in this study.

Gene	Primer Sequence	Accession No
mouse iNOS	Forward 5′-GCATCCCTGTGGAGGACAACC-3′ Reverse 5′-GCATCCCTGTGGAGGACAACC-3′	M20234
mouse TNF-α	Forward 5′-GCATCCCTGTGGAGGACAACC-3′ Reverse 5′-AAGACGCTGCACTGCTGGTC-3′	BC076598
mouse IL-6	Forward 5′-TCTGGCCTCCAGTTACCAAC-3′ Reverse 5′-TCAGTGAGGAGAGGCTGGTT-3′	EU554632
mouse GAPDH	Forward 5′-GCGAGACCCCACTAACATCA-3′ Reverse 5′-GAGTTGGGATAGGGCCTCTCTT-3′	GU214026

4.10. COX-1/2 Inhibition Assay

The inhibitory activity of each COX-1/2 ligand was detected using a COX-1/2 Inhibitor Screening Kit (BioVison, Milpitas, CA, USA). COX Assay Buffer (75 μL), COX Cofactor working solution (2 μL), COX probe solution (1 μL), recombinant COX-1 or COX-2 (1 μL), arachidonic acid/NAOH solution (10 μL), and test solution (10 μL) were mixed in a 96-well plate, and fluorescence kinetics were measured for 10 min at 25 °C. The fluorescence value of each well was measured with an excitation wavelength of 535 nm and an emission wavelength of 587 nm. Celecoxib, a COX-2 inhibitor, was used as the positive control group. Two points (T_1 and T_2) in the linear range of the plot were used to obtain the corresponding fluorescence values (RFU_1 and RFU_2). Then, the slope for all samples (S) was calculated by dividing the net ΔRFU ($RFU_2 - RFU_1$) values by the time ΔT ($T_2 - T_1$) as follows in Equation (2):

$$\text{Relative inhibition (\%)} = (\text{slope of the Enzyme Control} - \text{slope of S})/(\text{slope of Enzyme Control}) \times 100 \quad (2)$$

The concentration of the test compound causing 50% inhibition (IC_{50}, μM) was calculated from the concentration inhibition response curve. The selectivity indices (SI, COX-1 IC_{50}/COX-2 IC_{50}) were also calculated and compared with that of the standard COX-2 selective inhibitor, celecoxib.

4.11. Molecular Docking

The AutoDock Vina program [58] was used to simulate COX-2 and SNAH docking, and celecoxib as a positive control. The docking pocket was previously identified in active sites of COX-2 complexes (PDB ID: 6COX). To prepare the docking simulation, the 3D structures of SNAH (Pubchem CID: 5280802) and celecoxib (Pubchem CID: 2662) were downloaded from PubChem (https://pubchem.ncbi.nlm.nih.gov/). Images of complexes and hydrogen bond predictions were obtained using Chimera version 1.14 (https://www.cgl.ucsf.edu/chimera/).

4.12. Statistical Analysis

Data are expressed as the mean ± standard deviation from three independent experiments. Statistical significance was determined by Student's t-test for independent means using Microsoft Excel. Data are presented as the mean ± SD of three independent experiments; $p < 0.05$ was considered statistically significant.

5. Conclusions

The results presented here demonstrate that SNAH exerted potent anti-inflammatory effects on RAW 264.7 macrophages. Treatment of LPS-stimulated RAW 264.7 macrophages with SNAH significantly attenuated the production of NO, TNF-α, and IL-6 by reducing their corresponding gene expression. The SNAH as a natural product had meaningful IC_{50} value to inhibit COX-2 and possible mode of action in the same pocket with celecoxib. The ability of SNAH to inhibit the inflammatory response was associated with a reduction of intracellular ROS production. The results of this study

support the use of SNAH as an alternative candidate for safe and effective treatment of inflammatory diseases. Further studies are needed to understand the precise molecular mechanisms regulating the anti-inflammatory activity in the animal model and validate it as a modulator of macrophage activation.

Author Contributions: D.P. and S.-H.B. designed the study. S.-H.B. performed the experiment and analyzed the data. T.P. and M.-G.K. performed molecular docking. S.-H.B., M.-G.K., T.P., and D.P. wrote the paper. S.-H.B., T.P., C.M.P., and D.P. revised the paper. All authors have read and agreed to the published version of the manuscript.

Funding: The research was supported by the National Research Foundation of Korea (NRF) funded by the Korean government (2018R1D1A1B07046744) and the National Research Council of Science & Technology grant by the Korea government (CRC-16–01-KRICT).

Conflicts of Interest: The authors declare no conflict of interest

Abbreviations

LPS	Lipopolysaccharide
NO	Nitric oxide
ROS	Reactive oxygen species
DPPH	2,2-diphenyl-1- picrylhydrazyl
TNF	Tumor necrosis factor
iNOS	Inducible nitric oxide synthase
eNOS	Endothelial NOS
nNOS	Neuronal NOS
COX-2	Cyclooxygenase-2
SI	Selectivity indices
ELISA	Enzyme-linked immunosorbent assay
TLR	Toll-like receptor
DCF-DA	2,7-dichlorofluorescein diacetate
DMEM	Dulbecco's Modified Eagle's Medium
SAPK/JNK	Stress-activated protein kinase/Jun-amino-terminal kinase
RIPA	Radioimmunoprecipitation assay

References

1. Riera-Romo, M.; Pérez-Martínez, D.; Ferrer, C.C. Innate immunity in vertebrates: An overview. *Immunology* **2016**, *148*, 125–139. [CrossRef] [PubMed]
2. Moriya, J. Critical roles of inflammation in atherosclerosis. *J. Cardiol.* **2019**, *73*, 22–27. [CrossRef] [PubMed]
3. Hansson, G.K. Inflammation, Atherosclerosis, and Coronary Artery Disease. *N. Engl. J. Med.* **2005**, *352*, 1685–1695. [CrossRef] [PubMed]
4. Kleinjan, A. Airway inflammation in asthma: Key players beyond the Th2 pathway. *Curr. Opin. Pulm. Med.* **2016**, *22*, 46–52. [CrossRef] [PubMed]
5. Dandona, P.; Aljada, A.; Bandyopadhyay, A. Inflammation: The link between insulin resistance, obesity and diabetes. *Trends Immunol.* **2004**, *25*, 4–7. [CrossRef]
6. Zeremski, M.; Petrovic, L.M.; Talal, A.H. The role of chemokines as inflammatory mediators in chronic hepatitis C virus infection. *J. Viral Hepat.* **2007**, *14*, 675–687. [CrossRef]
7. Liu, S.F.; Malik, A.B. NF-κB activation as a pathological mechanism of septic shock and inflammation. *Am. J. Physiol. Cell. Mol. Physiol.* **2006**, *290*, L622–L645. [CrossRef]
8. Zipp, F.; Aktas, O. The brain as a target of inflammation: Common pathways link inflammatory and neurodegenerative diseases. *Trends Neurosci.* **2006**, *29*, 518–527. [CrossRef]
9. Abdulkhaleq, L.A.; Assi, M.A.; Abdullah, R.; Zamri-Saad, M.; Taufiq-Yap, Y.H.; Hezmee, M.N.M. The crucial roles of inflammatory mediators in inflammation: A review. *Veter World* **2018**, *11*, 627–635. [CrossRef]
10. Noailles, A.; Maneu, V.; Campello, L.; Lax, P.; Cuenca, N. Systemic inflammation induced by lipopolysaccharide aggravates inherited retinal dystrophy. *Cell Death Dis.* **2018**, *9*, 1–18. [CrossRef]
11. Shin, W.-B.; Dong, X.; Kim, Y.-S.; Park, J.-S.; Kim, S.-J.; Go, E.-A.; Kim, E.-K.; Park, P.-J. Anti-inflammatory Effects of *Batillaria multiformis* Water Extracts via NF-κB and MAPK Signaling Pathways in LPS-Induced RAW 264.7 Cells. *Adv. Exp. Med. Biol.* **2019**, *1155*, 1001–1014. [CrossRef] [PubMed]

12. Diao, J.; Chi, Z.; Guo, Z.; Zhang, L. Mung Bean Protein Hydrolysate Modulates the Immune Response Through NF-κB Pathway in Lipopolysaccharide-Stimulated RAW 264.7 Macrophages. *J. Food Sci.* **2019**, *84*, 2652–2657. [CrossRef] [PubMed]
13. Jeong, Y.H.; Oh, Y.-C.; Cho, W.-K.; Yim, N.-H.; Ma, J.Y. Hoveniae Semen Seu Fructus Ethanol Extract Exhibits Anti-Inflammatory Activity via MAPK, AP-1, and STAT Signaling Pathways in LPS-Stimulated RAW 264.7 and Mouse Peritoneal Macrophages. *Mediat. Inflamm.* **2019**, *2019*, 9184769. [CrossRef] [PubMed]
14. Kim, T.-W.; Shin, J.-S.; Chung, K.-S.; Lee, Y.-G.; Baek, N.-I.; Lee, K.-T. Anti-Inflammatory Mechanisms of Koreanaside A, a Lignan Isolated from the Flower of *Forsythia koreana*, against LPS-Induced Macrophage Activation and DSS-Induced Colitis Mice: The Crucial Role of AP-1, NF-κB, and JAK/STAT Signaling. *Cells* **2019**, *8*, 1163. [CrossRef]
15. Lobo, V.; Patil, A.; Phatak, A.; Chandra, N. Free radicals, antioxidants and functional foods: Impact on human health. *Pharmacogn. Rev.* **2010**, *4*, 118–126. [CrossRef]
16. Pizzino, G.; Irrera, N.; Cucinotta, M.; Pallio, G.; Mannino, F.; Arcoraci, V.; Squadrito, F.; Altavilla, D.; Bitto, A. Oxidative Stress: Harms and Benefits for Human Health. *Oxidative Med. Cell. Longev.* **2017**, *2017*, 1–13. [CrossRef]
17. Johar, R.; Sharma, R.; Kaur, A.; Mukherjee, T.K. Role of Reactive Oxygen Species in Estrogen Dependant Breast Cancer Complication. *Anti-Cancer Agents Med. Chem.* **2015**, *16*, 190–199. [CrossRef]
18. Priya, L.B.; Baskaran, R.; Huang, C.-Y.; Padma, V.V. Neferine ameliorates cardiomyoblast apoptosis induced by doxorubicin: Possible role in modulating NADPH oxidase/ROS-mediated NFκB redox signaling cascade. *Sci. Rep.* **2017**, *7*, 12283. [CrossRef]
19. Qi, S.; Feng, Z.; Li, Q.; Qi, Z.; Zhang, Y. Myricitrin Modulates NADPH Oxidase-Dependent ROS Production to Inhibit Endotoxin-Mediated Inflammation by Blocking the JAK/STAT1 and NOX2/p47phoxPathways. *Oxidative Med. Cell. Longev.* **2017**, *2017*, 1–20. [CrossRef]
20. Wu, X.; Gao, H.; Hou, Y.; Yu, J.; Sun, W.; Wang, Y.; Chen, X.; Feng, Y.; Xu, Q.-M.; Chen, X. Dihydronortanshinone, a natural product, alleviates LPS-induced inflammatory response through NF-κB, mitochondrial ROS, and MAPK pathways. *Toxicol. Appl. Pharmacol.* **2018**, *355*, 1–8. [CrossRef]
21. Farah, M.; Samuelsson, G. Pharmacologically Active Phenylpropanoids from *Senra incana*. *Planta Medica* **1992**, *58*, 14–18. [CrossRef] [PubMed]
22. Kim, H.; Lee, J.S.; Sezirahiga, J.; Kwon, J.; Jeong, M.; Lee, D.; Choi, J.-H.; Jang, D.S. A New Canthinone-Type Alkaloid Isolated from *Ailanthus altissima* Swingle. *Molecules* **2016**, *21*, 642. [CrossRef]
23. Conde, E.; Cadahia, E.; Garcia-Vallejo, M.C.; Tomas-Barberan, F. Low molecular weight polyphenols in wood and bark of *Eucalyptus globulus*. *Wood Fiber Sci.* **2007**, *27*, 379–383.
24. Koshiba, T.; Hirose, N.; Mukai, M.; Yamamura, M.; Hattori, T.; Suzuki, S.; Sakamoto, M.; Umezawa, T. Characterization of 5-Hydroxyconiferaldehyde O-Methyltransferase in *Oryza sativa*. *Plant Biotechnol.* **2013**, *30*, 157–167. [CrossRef]
25. Zheng, L.-P.; He, Z.-G.; Wu, Z.-J.; Zhang, C. Chemical constituents from *Dendropanax dentiger*. *Chem. Nat. Compd.* **2012**, *48*, 883–885. [CrossRef]
26. Van Acker, R.; Déjardin, A.; Desmet, S.; Hoengenaert, L.; Vanholme, R.; Morreel, K.; Laurans, F.; Kim, H.; Santoro, N.; Foster, C.; et al. Different Routes for Conifer- and Sinapaldehyde and Higher Saccharification upon Deficiency in the Dehydrogenase CAD1. *Plant Physiol.* **2017**, *175*, 1018–1039. [CrossRef]
27. Meerungrueang, W.; Panichayupakaranant, P. Antimicrobial activities of some Thai traditional medical longevity formulations from plants and antibacterial compounds from *Ficus foveolata*. *Pharm. Biol.* **2014**, *52*, 1104–1109. [CrossRef]
28. Bancos, S.; Tsai, D.-H.; Hackley, V.; Weaver, J.L.; Tyner, K.M. Evaluation of Viability and Proliferation Profiles on Macrophages Treated with Silica Nanoparticles In Vitro via Plate-Based, Flow Cytometry, and Coulter Counter Assays. *ISRN Nanotechnol.* **2012**, *2012*, 1–11. [CrossRef]
29. Liang, Y.-C.; Huang, Y.T.; Tsai, S.-H.; Lin-Shiau, S.-Y.; Chen, C.-F.; Lin, J.-K. Suppression of inducible cyclooxygenase and inducible nitric oxide synthase by apigenin and related flavonoids in mouse macrophages. *Carcinog.* **1999**, *20*, 1945–1952. [CrossRef]
30. Hu, W.; Wang, X.-F.; Wu, L.; Shen, T.; Ji, L.; Zhao, X.; Si, C.-L.; Jiang, Y.; Wang, G. Apigenin-7-O-β-d-glucuronide inhibits LPS-induced inflammation through the inactivation of AP-1 and MAPK signaling pathways in RAW 264.7 macrophages and protects mice against endotoxin shock. *Food Funct.* **2016**, *7*, 1002–1013. [CrossRef]

31. Ji, G.; Zhang, Y.; Yang, Q.; Cheng, S.; Hao, J.; Zhao, X.; Jiang, Z. Genistein Suppresses LPS-Induced Inflammatory Response through Inhibiting NF-κB following AMP Kinase Activation in RAW 264.7 Macrophages. *PLoS ONE* **2012**, *7*, e53101. [CrossRef] [PubMed]
32. Abdel-Aziz, A.A.-M.; El-Azab, A.S.; A Abou-Zeid, L.; Eltahir, K.E.H.; Abdel-Aziz, N.; Ayyad, R.R.; Al-Obaid, A.M. Synthesis, anti-inflammatory, analgesic and COX-1/2 inhibition activities of anilides based on 5,5-diphenylimidazolidine-2,4-dione scaffold: Molecular docking studies. *Eur. J. Med. Chem.* **2016**, *115*, 121–131. [CrossRef] [PubMed]
33. Skaper, S.D.; Facci, L.; Zusso, M.; Giusti, P. An Inflammation-Centric View of Neurological Disease: Beyond the Neuron. *Front. Cell. Neurosci.* **2018**, *12*, 72. [CrossRef] [PubMed]
34. Stephenson, J.; Nutma, E.; Van Der Valk, P.; Amor, S. Inflammation in CNS neurodegenerative diseases. *Immunol.* **2018**, *154*, 204–219. [CrossRef] [PubMed]
35. Paoletti, R.; Bolego, C.; Poli, A.; Cignarella, A. Metabolic syndrome, inflammation and atherosclerosis. *Vasc. Heal. Risk Manag.* **2006**, *2*, 145–152. [CrossRef] [PubMed]
36. Van Amersfoort, E.S.; Van Berkel, T.J.C.; Kuiper, J. Receptors, Mediators, and Mechanisms Involved in Bacterial Sepsis and Septic Shock. *Clin. Microbiol. Rev.* **2003**, *16*, 379–414. [CrossRef] [PubMed]
37. A Wink, D.; Hines, H.B.; Cheng, R.Y.S.; Switzer, C.H.; Flores-Santana, W.; Vitek, M.P.; Ridnour, L.A.; Colton, C.A. Nitric oxide and redox mechanisms in the immune response. *J. Leukoc. Biol.* **2011**, *89*, 873–891. [CrossRef]
38. Muniandy, K.; Gothai, S.; Badran, K.M.H.; Kumar, S.S.; Esa, N.M.; Arulselvan, P. Suppression of Proinflammatory Cytokines and Mediators in LPS-Induced RAW 264.7 Macrophages by Stem Extract of *Alternanthera sessilis* via the Inhibition of the NF-κB Pathway. *J. Immunol. Res.* **2018**, *2018*, 1–12. [CrossRef]
39. Xiang, L.; Hu, Y.-F.; Wu, J.-S.; Wang, L.; Huang, W.-G.; Xu, C.-S.; Meng, X.-L.; Wang, P. Semi-Mechanism-Based Pharmacodynamic Model for the Anti-Inflammatory Effect of Baicalein in LPS-Stimulated RAW264.7 Macrophages. *Front. Pharmacol.* **2018**, *9*, 793. [CrossRef]
40. Lv, Y.; Hu, S.; Lu, J.; Dong, N.; Liu, Q.; Du, M.; Zhang, H. Upregulating Nonneuronal Cholinergic Activity Decreases TNF Release from Lipopolysaccharide-Stimulated RAW264.7 Cells. *Mediat. Inflamm.* **2014**, *2014*, 1–10. [CrossRef]
41. Förstermann, U.; Sessa, W. Nitric oxide synthases: Regulation and function. *Eur. Hear. J.* **2011**, *33*, 829–837. [CrossRef] [PubMed]
42. Lowry, J.L.; Brovkovych, V.; Zhang, Y.; Skidgel, R.A. Endothelial Nitric-oxide Synthase Activation Generates an Inducible Nitric-oxide Synthase-like Output of Nitric Oxide in Inflamed Endothelium*. *J. Biol. Chem.* **2012**, *288*, 4174–4193. [CrossRef] [PubMed]
43. Xue, Q.; Yan, Y.; Zhang, R.; Xiong, H. Regulation of iNOS on Immune Cells and Its Role in Diseases. *Int. J. Mol. Sci.* **2018**, *19*, 3805. [CrossRef] [PubMed]
44. Zidar, N.; Odar, K.; Glavač, D.; Jerše, M.; Zupanc, T.; Štajer, D. Cyclooxygenase in normal human tissues – is COX-1 really a constitutive isoform, and COX-2 an inducible isoform? *J. Cell. Mol. Med.* **2008**, *13*, 3753–3763. [CrossRef]
45. Nørregaard, R.; Kwon, T.-H.; Frøkiær, J. Physiology and pathophysiology of cyclooxygenase-2 and prostaglandin E2 in the kidney. *Kidney Res. Clin. Pract.* **2015**, *34*, 194–200. [CrossRef]
46. Hsieh, I.-N.; Chang, A.S.-Y.; Teng, C.-M.; Chen, C.-C.; Yang, C.-R. Aciculatin inhibits lipopolysaccharide-mediated inducible nitric oxide synthase and cyclooxygenase-2 expression via suppressing NF-κB and JNK/p38 MAPK activation pathways. *J. Biomed. Sci.* **2011**, *18*, 28. [CrossRef]
47. Park, J.-W.; Kwon, O.-K.; Kim, J.-H.; Oh, S.-R.; Kim, J.-H.; Paik, J.-H.; Marwoto, B.; Widjhati, R.; Juniarti, F.; Irawan, D.; et al. Rhododendron album Blume inhibits iNOS and COX-2 expression in LPS-stimulated RAW264.7 cells through the downregulation of NF-?B signaling. *Int. J. Mol. Med.* **2015**, *35*, 987–994. [CrossRef]
48. Kwon, D.H.; Cha, H.-J.; Choi, E.O.; Leem, S.-H.; Kim, G.-Y.; Moon, S.-K.; Chang, Y.-C.; Yun, S.-J.; Hwang, H.J.; Kim, B.W.; et al. Schisandrin A suppresses lipopolysaccharide-induced inflammation and oxidative stress in RAW 264.7 macrophages by suppressing the NF-κB, MAPKs and PI3K/Akt pathways and activating Nrf2/HO-1 signaling. *Int. J. Mol. Med.* **2017**, *41*, 264–274. [CrossRef]
49. Schieber, M.; Chandel, N.S. ROS Function in Redox Signaling and Oxidative Stress. *Curr. Biol.* **2014**, *24*, R453–R462. [CrossRef]

50. Forrester, S.J.; Kikuchi, D.S.; Hernandes, M.S.; Xu, Q.; Griendling, K.K. Reactive Oxygen Species in Metabolic and Inflammatory Signaling. *Circ. Res.* **2018**, *122*, 877–902. [CrossRef]
51. Zhang, J.; Wang, X.; Vikash, V.; Ye, Q.; Wu, D.; Liu, Y.; Dong, W. ROS and ROS-Mediated Cellular Signaling. *Oxidative Med. Cell. Longev.* **2016**, *2016*, 1–18. [CrossRef] [PubMed]
52. El-Zayat, S.R.; Sibaii, H.; Mannaa, F.A. Toll-like receptors activation, signaling, and targeting: An overview. *Bull. Natl. Res. Cent.* **2019**, *43*, 1–12. [CrossRef]
53. Hoesel, B.; Schmid, J. The complexity of NF-κB signaling in inflammation and cancer. *Mol. Cancer* **2013**, *12*, 86. [CrossRef] [PubMed]
54. Laird, M.H.W.; Rhee, S.H.; Perkins, D.J.; Medvedev, A.E.; Piao, W.; Fenton, M.J.; Vogel, S.N. TLR4/MyD88/PI3K interactions regulate TLR4 signaling. *J. Leukoc. Biol.* **2009**, *85*, 966–977. [CrossRef] [PubMed]
55. Limongelli, V.; Bonomi, M.; Marinelli, L.; Gervasio, F.L.; Cavalli, A.; Novellino, E.; Parrinello, M. Molecular basis of cyclooxygenase enzymes (COXs) selective inhibition. *Proc. Natl. Acad. Sci. USA* **2010**, *107*, 5411–5416. [CrossRef]
56. Sharma, V.; Bhatia, P.; Alam, O.; Naim, M.J.; Nawaz, F.; Sheikh, A.A.; Jha, M. Recent advancement in the discovery and development of COX-2 inhibitors: Insight into biological activities and SAR studies (2008–2019). *Bioorganic Chem.* **2019**, *89*, 103007. [CrossRef]
57. Ichikawa, K.; Sasada, R.; Chiba, K.; Gotoh, H. Effect of Side Chain Functional Groups on the DPPH Radical Scavenging Activity of Bisabolane-Type Phenols. *Antioxidants* **2019**, *8*, 65. [CrossRef]
58. Trott, O.; Olson, A.J. AutoDock Vina: Improving the speed and accuracy of docking with a new scoring function, efficient optimization, and multithreading. *J. Comput. Chem.* **2009**, *31*, 455–461. [CrossRef]

Sample Availability: All samples in these studies are available.